

Interpreting potential field data using continuous wavelet transforms of their horizontal derivatives

G.R.J. Cooper

School of Geosciences, University of the Witwatersrand, Johannesburg 2050, South Africa

Received 19 October 2005; accepted 20 October 2005

Abstract

The continuous wavelet transform has been used with much success in the analysis of non-stationary time series. It has been used much less frequently in the interpretation of magnetic or gravity data, although several approaches have been tried. A simple method of obtaining location and depth estimates of gravity and magnetic field sources is suggested here. For gravity data the method uses wavelets based on the integer-order horizontal derivatives of the gravity anomaly from a point source (the Poisson kernel). For magnetic data the wavelet is based on the integer-order horizontal derivatives of the analytic signal of the anomaly from a contact or a thin sheet. The method is compared with Euler deconvolution, and is demonstrated with synthetic models and on gravity and magnetic data from South Africa.

© 2005 Elsevier Ltd. All rights reserved.

Keywords: Euler deconvolution; Magnetics; Gravity; Semi-automatic interpretation

1. Introduction

Wavelets are a powerful tool for analysing the properties of a data set as a function of both time (or position) and scale (which is related to wavelength). The transform uses a wavelet Ψ as its basis function. To be admissible as a wavelet a function must have a zero mean. The continuous wavelet transform (CWT) is obtained by correlating scaled versions of the wavelet with the data f (Mallat, 1998, p.5)

$$Wf(u, s) = \int_{-\infty}^{\infty} f(t) \frac{1}{\sqrt{s}} \Psi^* \left(\frac{t-u}{s} \right) dt, \quad (1)$$

where s is scale and u is position.

Most applications of wavelets to potential field data used wavelets derived from the Poisson kernel (Moreau et al., 1999), which is based on the gravity anomaly from a point source. In that case it is possible to achieve the scaling of the wavelet in Eq. (1) with an upward continuation operation. When data profiles are being analysed the model is assumed to be two dimensional, and the anomaly and its derivatives are based on the buried cylinder response and its derivatives (Beck, 1981 p.79);

$$g = \frac{Gmz}{(x^2 + z^2)}. \quad (2)$$

When used as the basis for a family of wavelets, G and m are not needed and z is set to one. Fig. 1 shows the gravity anomaly from a buried cylinder and its first and second horizontal derivatives. The derivatives are suitable as wavelets while the

E-mail address: cooperg@geosciences.wits.ac.za.

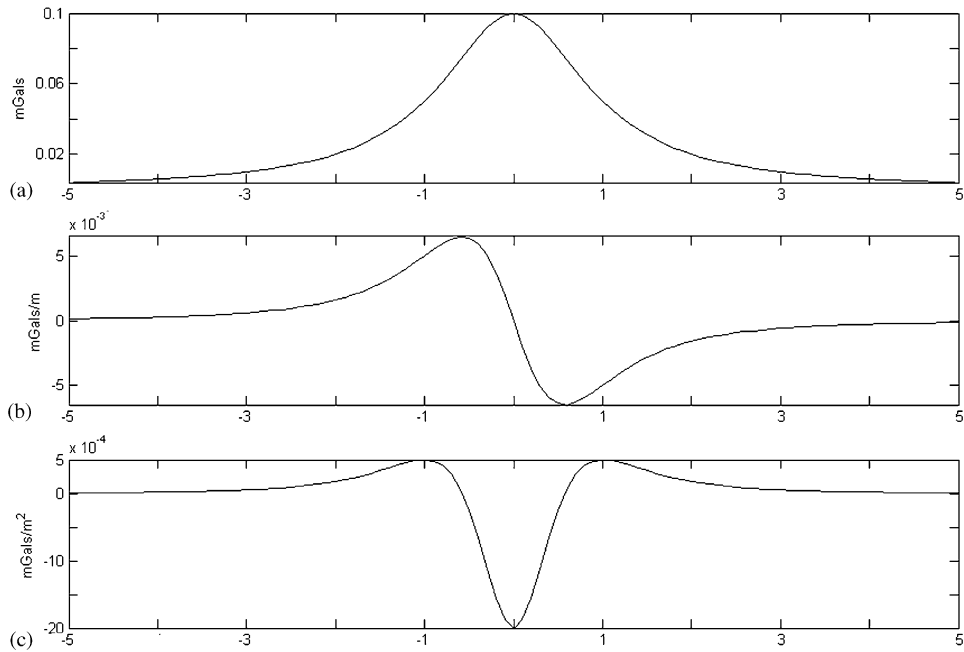


Fig. 1. (a) Gravity anomaly over a horizontal cylinder, calculated using Eq. (2). (b) First horizontal derivative of gravity anomaly over a horizontal cylinder, calculated using Eq. (3). (c) Second horizontal derivative of gravity anomaly over a horizontal cylinder, calculated using Eq. (4).

anomaly itself is not, because it does not have a zero mean. The derivatives of Eq. (2) are:

$$\frac{\partial g}{\partial x} = \frac{-2Gmzx}{(x^2 + z^2)^2}, \quad (3)$$

$$\frac{\partial^2 g}{\partial x^2} = \frac{2Gmz(3x^2 - z^2)}{(x^2 + z^2)^3}. \quad (4)$$

2. Background and application of wavelets to gravity data

There have been many papers published on the application of wavelets to potential field data. Fedi and Quarta (1998) used the discrete wavelet transform to perform regional-residual separation. Ridsdill-Smith and Dentith (1999) computed cleaner derivatives of aeromagnetic data using the wavelet transform. Moreau et al. (1999) analysed maxima in the modulus of the CWT of gravity and magnetic data as a guide to source depth determination. They also determined the degree of source homogeneity from the decay in amplitude of the wavelet coefficients. Sailhac et al. (2000) extended this approach to include complex wavelets, and applied it to mag-

netic data. Their approach did not require the prior reduction of the data to the pole or equator before wavelet processing. Martelet et al. (2001) took a similar approach and applied it to gravity data from Nepal. Boschetti et al. (2001) delineated the edges and dip of sources by looking at the location of local maxima of the upward continued field. Leblanc and Morris (2001) used the discrete wavelet transform to denoise aeromagnetic data, while de Oliveira Lyrio et al. (2004) used it to denoise gravity gradiometry data. Valee et al. (2004) used complex wavelets to analyse magnetic data. They estimated source depth from a ratio of the first- and second-order wavelet coefficients.

This paper takes a different approach to those discussed above. When applying the method, the data is first differentiated by the same degree as the wavelet order. For example, if the wavelet used is based on the first horizontal derivative of the gravity anomaly from a cylinder (Eq. (3)), then the CWT is applied to the first horizontal derivative of the data. The CWT then becomes a cross-correlation between the wavelet and the data, and source locations and depths may be read directly from the CWT plot. Fig. 2 shows the application of this type of wavelet analysis to gravity data from a simple model. The gravity response of the model is shown

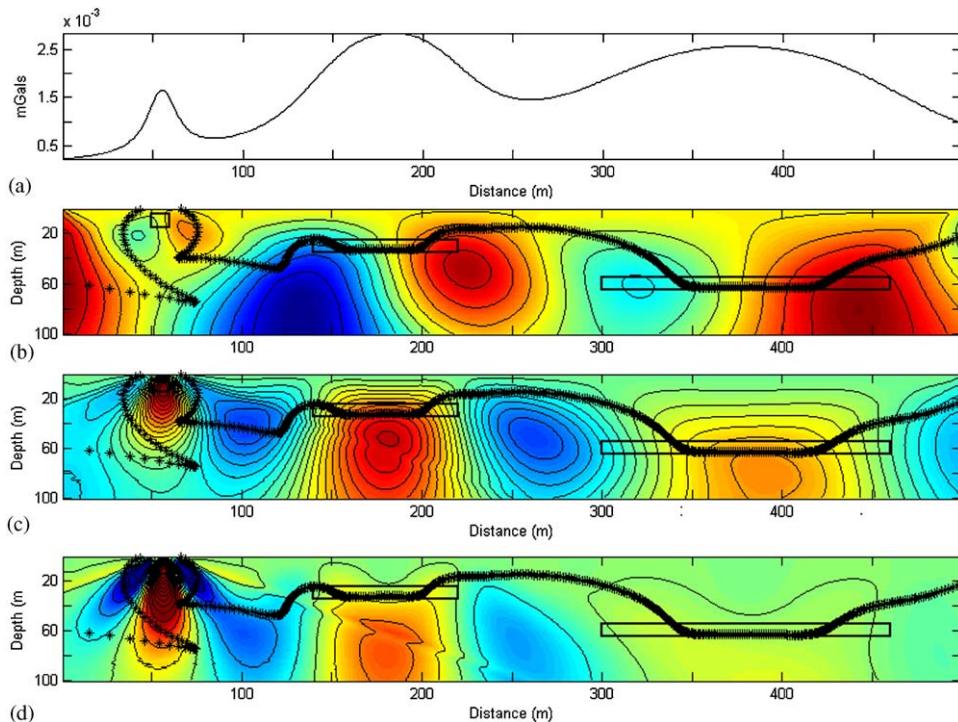


Fig. 2. (a) Gravity anomaly produced by bodies (shown as black rectangles in Figs. 2b–d). (b) CWT analysis using a wavelet based on Eq. (3) applied to data in Fig. 2(a). Light shades correspond to a strong positive response while dark shades correspond to a strong negative response. In Figs. 2b–d + symbols correspond to Euler deconvolution solutions. SI used was 1.0 and window size was 11 points. All solutions are plotted. (c) CWT analysis using a wavelet based on Eq. (3) applied to first horizontal derivative of data in Fig. 2a. (d) CWT analysis using a wavelet based on Eq. (4) applied to second horizontal derivative of data in Fig. 2a.

in Fig. 2a, while the model itself is overlain on the CWT in Figs. 2b–d. In Fig. 2b the CWT has been calculated directly from the data using a wavelet based on Eq. (3). The result is not promising, with little obvious correlation between the body locations and the maxima or minima of the CWT plot. However when the CWT of the first horizontal derivative of the data was calculated (again using a wavelet based on Eq. (3)) the plot shows maxima located on or near the bodies (Fig. 2c). The resolution of the result becomes poorer as the body depth increases, as would be expected. When the CWT of the second horizontal derivative of the data was calculated using a wavelet based on Eq. (4) this provided improved source location for the shallower bodies, but the response from the deeper body is degraded due to the second horizontal derivative operation removing the longer wavelength content of the signal, and hence the information about the deeper sources.

Overlain on all the CWT plots is the Euler deconvolution response. Euler deconvolution is a commonly used first step in the interpretation of

magnetic data. It analyses potential field data in terms of simple magnetic or gravity distributions such as point poles or dipoles. These different source types are described by a factor known as the structural index which gives the rate of decay of the amplitude of the field with distance from the source. Euler deconvolution passes a moving window through the data and uses least-squares inversion to obtain the depth and horizontal location of sources with different structural indices (Thomson, 1982; Reid et al., 1990). The Euler solutions from the data in Fig. 2a correlate well with the results of the CWT analysis. Euler deconvolution can also be applied to the vertical derivative of potential field data (Stavrev, 1997), which can give improved source location if the data noise levels allow. For the CWT analysis to be applied to the vertical derivative of the field, the wavelets used must be based on the horizontal derivatives of the vertical derivative of the gravity function in Eq. (2), i.e.

$$\frac{\partial^2 g}{\partial z \partial x} = \frac{-2Gmx(x^2 - 3z^2)}{(x^2 + z^2)^3}, \quad (5)$$

$$\frac{\partial^3 g}{\partial z \partial x^2} = \frac{6Gm(x^4 - 6x^2z^2 + z^4)}{(x^2 + z^2)^4}. \quad (6)$$

The use of higher derivatives obviously makes the method susceptible to noise (as will be discussed in more detail below), but noise is a problem for Euler deconvolution also. Fig. 3 shows CWT plots of the horizontal derivatives of the first vertical derivative of the gravity data. As expected, the responses from the deeper bodies are further degraded compared with Fig. 2, but the CWT maxima over the shallower bodies appears sharper. The location of the Euler deconvolution solutions from the first vertical derivative of the data is much improved compared to that shown in Fig. 2.

Fig. 4 shows the CWT response (using the first horizontal derivative wavelet) and Euler solutions for a model consisting of three dyke-like bodies at different depths. In Figs. 4c and d 5% and 15% uniformly distributed random noise, respectively, was added to the data prior to the CWT and Euler calculations. It might be thought that the noise, being composed of short wavelengths compared to

the signal, would appear only in the smaller scales (corresponding to shallow depths) of the CWT. However due to the ‘cone of influence’ effect (Mallat, 1998, p.175) there is a noticeable effect at larger scales as well, although the overall structure of the CWT is not seriously disturbed even by 15% random noise—a level (hopefully) far exceeding that likely to be encountered in practice. By comparison the Euler solutions have collapsed completely to shallow depths at this noise level.

The Trompsburg gravity anomaly from the Free State province, South Africa is shown in Fig. 5. The anomaly was first discovered by B.D. Maree in 1942, and Buchmann later performed a detailed gravity survey (Buchmann, 1960). The anomaly is a gravity high of 100mGals amplitude, and may be caused by a granite sill. The CWT plots (based on wavelets derived from the horizontal derivatives of the gravity anomaly from a point source, rather than a cylinder, due to the 3D nature of the anomaly) locate a source at a depth 20–40 km, which agrees with the Euler deconvolution solutions.

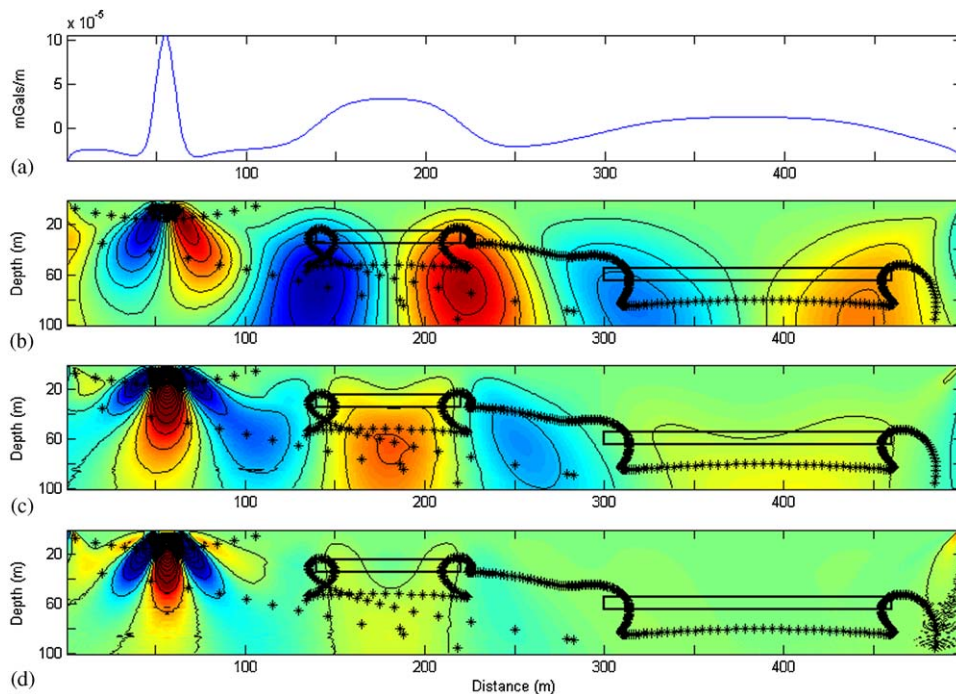


Fig. 3. (a) First vertical derivative of gravity anomaly produced by bodies (shown as black rectangles) in Figs. 3b–d. (b) CWT analysis using a wavelet based on Eq. (5) applied to data in Fig. 3(a). Light shades correspond to a strong positive response while dark shades correspond to a strong negative response. In Figs. 3b–d + symbols correspond to Euler deconvolution solutions. SI used was 2.0 and window size was 11 points. All solutions are plotted. (c) CWT analysis using a wavelet based on Eq. (5) applied to first horizontal derivative of data in Fig. 3a. (d) CWT analysis using a wavelet based on Eq. (6) applied to second horizontal derivative of data in Fig. 3a.

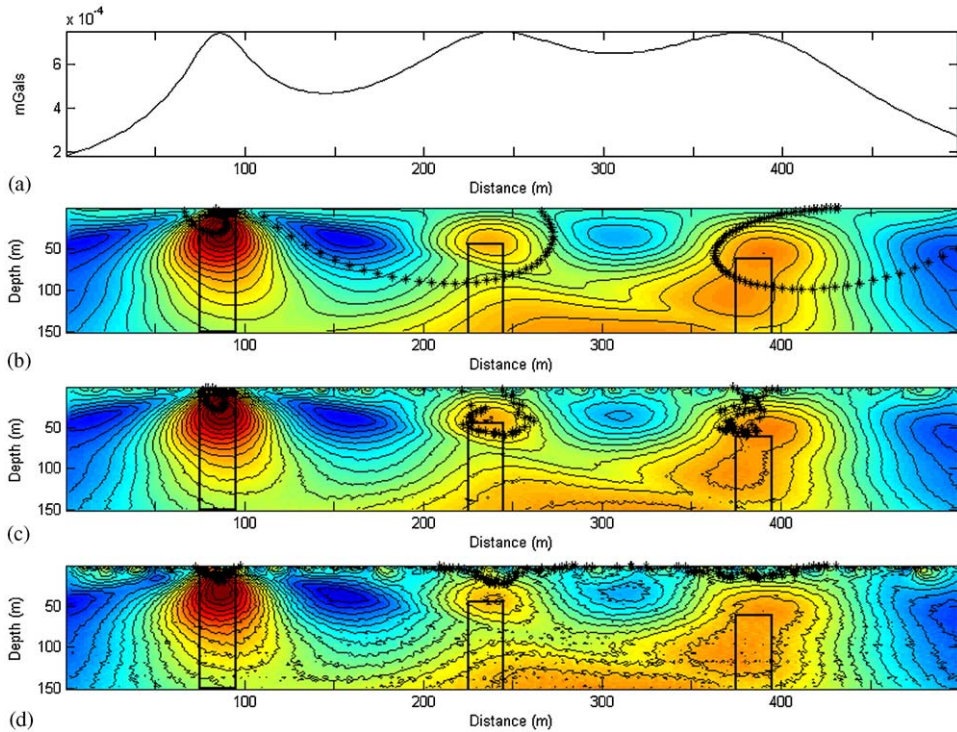


Fig. 4. (a) Gravity anomaly produced by bodies (shown as black rectangles) in Figs. 4b–d. (b) CWT analysis using a wavelet based on Eq. (3) applied to first horizontal derivative of data in Fig. 4(a). Light shades correspond to a strong positive response while dark shades correspond to a strong negative response. In Figs. 4b–d + symbols correspond to Euler deconvolution solutions. SI used was 1.0 and window size was 11 points. All solutions are plotted. (c) CWT analysis using a wavelet based on Eq. (3) applied to first horizontal derivative of data in Fig. 4(a). Uniformly distributed random noise of amplitude equal to 5% of maximum data amplitude was added before CWT analysis was performed. (d) CWT analysis using a wavelet based on Eq. (3) applied to first horizontal derivative of data in Fig. 4(a). Uniformly distributed random noise of amplitude equal to 15% of maximum data amplitude was added before CWT analysis was performed.

3. Application to magnetic data

With magnetic data two families of mother wavelets are discussed here, based on the horizontal derivatives of the analytic signal of the anomaly from two models, namely the contact and the thin dyke. The analytic signal across a contact is given by (Nabighian, 1972)

$$As_{con} = \frac{2kFc \sin d}{(x^2 + z^2)^{0.5}}, \quad (7)$$

where k is the susceptibility, F is the geomagnetic field intensity, $c = 1 - \cos^2 i \sin^2 A$, d is dip, i is the geomagnetic inclination, and A is the angle between magnetic North and the profile azimuth. The first and second horizontal derivatives of (7) are then

$$\frac{\partial As_{con}}{\partial x} = \frac{-2xkFc \sin d}{(x^2 + z^2)^{1.5}} \quad (8)$$

and

$$\frac{\partial^2 As_{con}}{\partial x^2} = \frac{2kFc \sin d(2x^2 - z^2)}{(x^2 + z^2)^{2.5}}. \quad (9)$$

When used as wavelets, the $2kFc \sin d$ terms are dropped. The wavelets based on Eqs. (8) and (9) are plotted in Fig. 6. The analytic signal across a thin sheet is (Keating and Pilkington, 2004)

$$As_{sheet} = \frac{2kFcw}{(x^2 + z^2)} \quad (10)$$

so that its first and second horizontal derivatives are:

$$\frac{\partial As_{sheet}}{\partial x} = \frac{-4xkFcw}{(x^2 + z^2)^2} \quad (11)$$

and

$$\frac{\partial^2 As_{sheet}}{\partial x^2} = \frac{2kFcw(3x^2 - z^2)}{(x^2 + z^2)^3}. \quad (12)$$

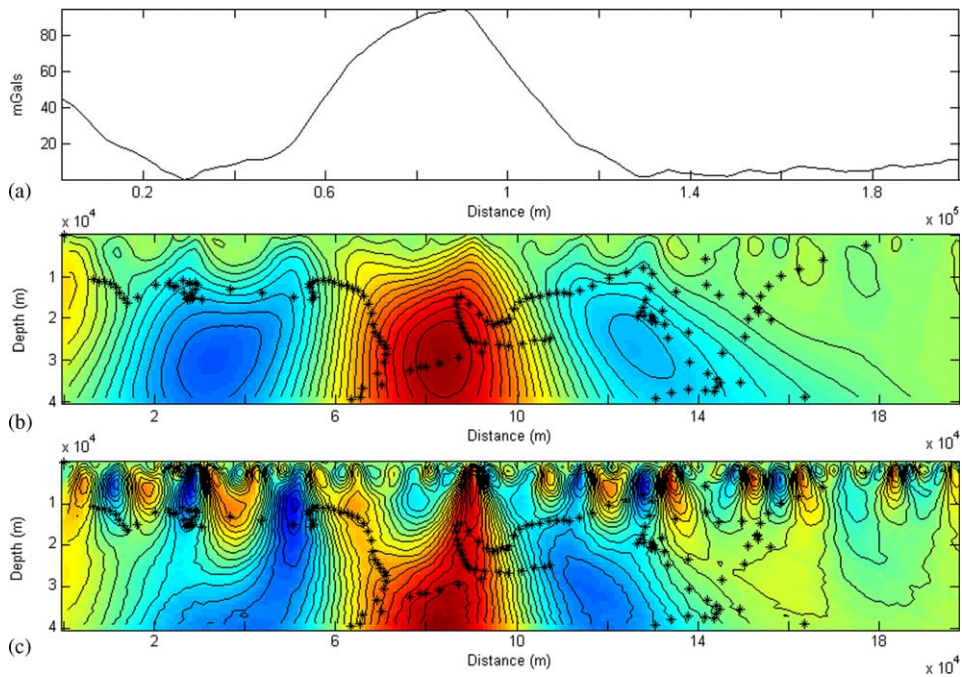


Fig. 5. (a) Gravity anomaly over Trompsburg structure, Free State province, South Africa. (b) CWT analysis of first horizontal derivative of data in Fig. 5a. In Figs. 5b and c + symbols correspond to Euler deconvolution solutions. SI used was 2.0 and window size was 21 points. All solutions are plotted. (c) CWT analysis of second horizontal derivative of data in Fig. 5a.

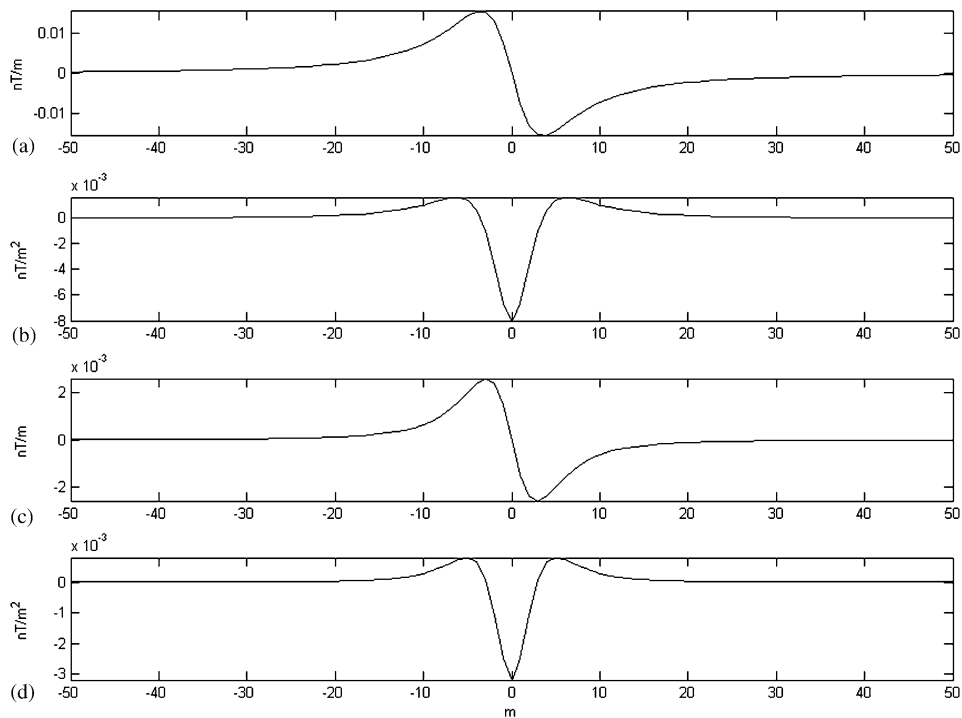


Fig. 6. (a) First horizontal derivative of analytic signal across a contact, as given by Eq. (8). (b) Second horizontal derivative of analytic signal across a contact, as given by Eq. (9). (c) First horizontal derivative of analytic signal across a sheet, as given by Eq. (11). (d) Second horizontal derivative of analytic signal across a sheet, as given by Eq. (12).

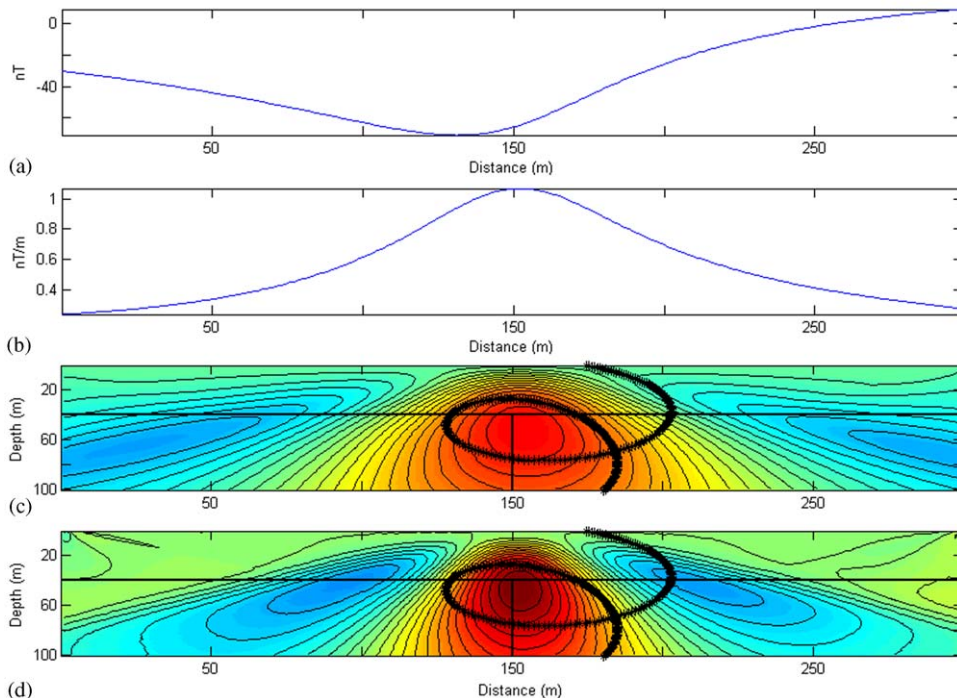


Fig. 7. (a). Magnetic anomaly over contact shown in Figs. 7b–d. Profile orientation was SN and field inclination used was -60° . (b) Analytic signal of data in Fig. 7a. (c) CWT analysis using a wavelet based on Eq. (8) applied to first horizontal derivative of analytic signal of data in Fig. 7a. In Figs. 7c and d + symbols correspond to Euler deconvolution solutions. SI used was 0.1 and window size was 11 points. All solutions are plotted. (d) CWT analysis using a wavelet based on Eq. (9) applied to second horizontal derivative of analytic signal of data in Fig. 7a.

The wavelets based on Eqs. (11) and (12) are also plotted in Fig. 6. As can be seen from a comparison of Figs. 1 and 6, all of the wavelets discussed here are similar in form and differ only subtly.

Fig. 7 shows the CWT analysis of data from a contact model using a wavelet based on Eq. (8), i.e. the first horizontal derivative of the analytic signal of the data is calculated, and the CWT analysis is applied to that. In Fig. 7d a wavelet based on Eq. (8) has been used and the CWT analysis applied to the second horizontal derivative of the analytic signal of the data. In both cases the maximum of the CWT plot occurs over the contact, with the resolution improving in the latter case.

Fig. 8 shows aeromagnetic data over a dyke in the Eastern Bushveld complex, South Africa. The dykes in this area are frequently remanent, and the palaeomagnetic studies and subsequent modelling required to produce the dyke model shown in the figure were performed by Mr. S. Letts of the School of Geosciences, University of the Witwatersrand. The CWT analyses, which used the wavelets based on Eq. (11) and (12), have maxima over the dyke

location. Although the data itself does not look noisy, the use of its higher derivatives produces a noisy CWT plot, although the maxima location is still clear. Euler deconvolution solutions are overlain on the plots for comparison once again, and their location correlates well with the CWT maxima.

4. Conclusions

CWT analysis using wavelets based on the horizontal derivatives of simple gravity and magnetic models can give useful information on the positions and depths of sources, providing the CWT is applied to the appropriate order of horizontal derivative of the data and not directly to the data itself. The technique was demonstrated on synthetic models and on gravity and magnetic data from South Africa.

Acknowledgements

The Council for Geoscience, Pretoria, is thanked for permission to use the gravity data over the

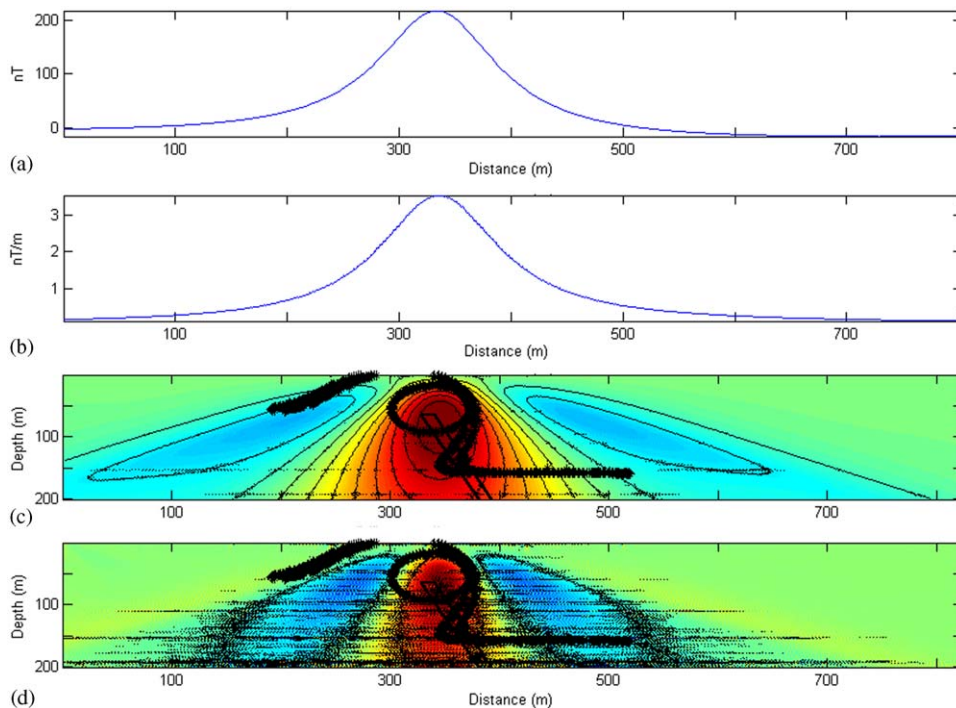


Fig. 8. (a) Magnetic profile across a dyke in Eastern Bushveld complex, South Africa. Flight height was 50 m and data were interpolated to a sample interval of 5 m. Field inclination at this location is -60° . (b) Analytic signal of data in Fig. 8a. (c) CWT analysis using a wavelet based on Eq. (10) applied to first horizontal derivative of analytic signal of data in Fig. 8a. In Figs. 8c and d + symbols correspond to Euler deconvolution solutions. SI used was 1.0 and window size was 11 points. All solutions are plotted. (d) CWT analysis using a wavelet based on Eq. (11) applied to second horizontal derivative of analytic signal of data in Fig. 8a.

Trompsburg anomaly. Mr. G. Chunnert of the AngloPlatinum corporation is thanked for permission to use the aeromagnetic data over the Bushveld complex, and Mr. S. Letts of the School of Geosciences, University of the Witwatersrand, is thanked for the use of his dyke model in Fig. 8.

References

- Beck, A.E., 1981. *Physical Principles of Exploration Methods*. Macmillan Press, New York, 234pp.
- Boschetti, F., Hornby, P., Horowitz, F.G., 2001. Wavelet based inversion of gravity data. *Exploration Geophysics* 32 (1), 48–55.
- Buchmann, J.P., 1960. Exploration of a geophysical anomaly at Trompsburg, orange free state, South Africa. *Transactions of the Geological Society of South Africa* 63, 1–10.
- de Oliveira Lyrio, J.C.S., Tenorio, L., Li, Y., 2004. Efficient automatic denoising of gravity gradiometry data. *Geophysics* 69 (3), 772–782.
- Fedi, M., Quarta, T., 1998. Wavelet analysis for the regional-residual and local separation of potential field anomalies. *Geophysical Prospecting* 46, 507–525.
- Keating, P., Pilkington, M., 2004. Euler deconvolution of the analytic signal and its application to magnetic interpretation. *Geophysical Prospecting* 52, 165–182.
- Leblanc, G.E., Morris, W.A., 2001. Denoising of aeromagnetic data via the wavelet transform. *Geophysics* (66), 1793–1804.
- Mallat, S., 1998. *A Wavelet Tour of Signal Processing*. Academic Press, New York, 577pp.
- Martelet, G., Sailhac, P., Moreau, F., Diament, M., 2001. Characterization of geological boundaries using 1-D wavelet transform on gravity data: theory and application to the Himalayas. *Geophysics* 66, 1116–1129.
- Moreau, F., Gilbert, D., Holschneider, M., Saracco, G., 1999. Identification of potential fields with the continuous wavelet transform: basic theory. *Journal of Geophysical Research* 104 (B3), 5003–5013.
- Nabighian, M.N., 1972. The analytic signal of two-dimensional magnetic bodies with polygonal cross-section: its properties and use for automated anomaly interpretation. *Geophysics* 37, 507–517.
- Reid, A.B., Allsop, J.M., Granser, H., Millet, A.J., Somerton, I.W., 1990. Magnetic interpretation in three dimensions using Euler deconvolution. *Geophysics* 55, 80–91.
- Ridsdill-Smith, T.A., Dentith, M.C., 1999. The wavelet transform in aeromagnetic processing. *Geophysics* 64, 1003–1013.
- Sailhac, P., Galdeano, A., Gibert, D., Moreau, F., Delor, C., 2000. Identification of sources of potential fields with the

- continuous wavelet transform: complex wavelets and application to aeromagnetic profiles in French Guiana. *Journal of Geophysical Research* 105, 19455–19475.
- Stavrev, P.Y., 1997. Euler deconvolution using differential similarity transformations of gravity or magnetic anomalies. *Geophysical Prospecting* 45, 207–246.
- Thomson, D.T., 1982. Eulph: A new technique for making computer assisted depth estimates from magnetic data. *Geophysics* 47 (1), 31–37.
- Valee, M.A., Keating, P., Smith, R.S., St-Hilaire, C., 2004. Estimating depth and model type using the continuous wavelet transform of magnetic data. *Geophysics* 69, 191–199.